

(Cr₂Hf)₂Al₃C₃- a proposed template for a new group of MAX-like materials

Yuxiang Mo¹, Sitaram Aryal, Paul Rulis, and Wai-Yim Ching

Department of Physics and Astronomy, University of Missouri-Kansas City,
Kansas City, Missouri 64110, USA

¹Electronic mail: yuxiangm@gmail.com

We predict the emergence of a new group of crystalline materials based on the template example of (Cr₂Hf)₂Al₃C₃. It has monoclinic symmetry with a $P2_1/m$ space group (#11), instead of $P6_3/mmc$ (#194) possessed by its progenitor, MAX phases. The lattice parameters of (Cr₂Hf)₂Al₃C₃ were found to be: $a = 5.1706 \text{ \AA}$, $b = 5.1945 \text{ \AA}$, $c = 12.8104 \text{ \AA}$; $\alpha = \beta = 90^\circ$, $\gamma = 119.8474^\circ$. The elastic properties and electronic structures are studied using the Vienna *Ab initio* Simulation Package and the first-principles orthogonalized linear combination of atomic orbitals method, respectively.

Keywords: MAX phase, crystal, space group

PACS number(s): 71.20.Be, 61.66.Dk

1. Introduction

The material under study, $(\text{Cr}_2\text{Hf})_2\text{Al}_3\text{C}_3$, is derived from Cr_2AlC which belongs to a large family of novel compounds: layered ternary transition-metal carbides and nitrides. The early discoveries (1-7) of these compounds (in powder form) date back to the 1960s. Three decades later, using a reactive hot-pressing method, Barsoum and El-Raghy (8) successfully fabricated single-phase Ti_3SiC_2 in polycrystalline bulk form, which enabled the observation of its unusual mechanical and transport properties. Such a development drew new attention to these carbides and nitrides, which have been extensively and intensively studied ever since (9, 10). The chemical compositions for most of these compounds can be summarized by a general formula: $\text{M}_{n+1}\text{AX}_n$ [M: an early transition-metal element, A: an A group (III, IV, V, or VI) element, X: carbon or nitrogen, and $n=1$ to 3], which is the reason why these compounds are also known as “MAX phases”. In a MAX phase, hexagonal near close-packed M, A, and X atoms form nanolaminated layered structures. Figure 1(a) shows the unit cell of Cr_2AlC , which is sometimes called a “(2 1 1)” phase because the stoichiometric ratio of the constituent elements is 2:1:1. MAX phases involve a hybrid of metallic, covalent, and ionic bonds (11) between the composing atoms. Very recently, we made available (12) quantitative bond order values for the various species of bonds in MAX phases using Mulliken analysis. This uncommon blend of bonding types in MAX phases has given these nanolaminated materials a very intricate and intriguing combination of properties. They are good conductors of heat and electricity. They are light-weight, stiff, and refractory, but also easily machinable. They can tolerate external damages and internal defects, as well as thermal shocks and high-temperature oxidation. Numerous ongoing and prospective applications of this remarkable group of materials range from cutting tools (13) and heat exchangers (14) all the way to high-end aerospace engineering applications such as coating materials on jet engine (15) (compressor and turbine) blades and spacecraft fuselages (16).

2. Crystal structures

2.1. The initial template

Interesting materials in relation to MAX phases have also been developed. Examples include ternary perovskite borides(17) and nitrides(18) (space group $Pm3m$, prototype CaTiO_3), Al_3BC_3 (19) (a metal borocarbide containing linear C-B-C units), orthorhombic Mo_2BC (20) (space group $Cmcm$), and the newly-discovered MXene(21) (2D nanosheets via exfoliation of MAX phase). Here, using $(\text{Cr}_2\text{Hf})_2\text{Al}_3\text{C}_3$ as an example, we demonstrate from a crystallographic point of view the possibility of incorporating more types of elements into a MAX phase while maintaining the crystallinity, instead of creating solid-solution phases. Such preservation of crystallinity could also preserve some tribological advantages(22, 23) and high electrical and thermal conductivities (due to the ease of electron and phonon scattering through periodic lattices). In the present work, the combination of Cr and Hf was used to study novel changes of properties because these two elements have such a large contrast of atomic radii and numbers of valence electrons. In practice, many other elements could be adopted for the combination, forming a large series (detailed later) of potential new materials. Figure 1 delineates how the crystal structure of $(\text{Cr}_2\text{Hf})_2\text{Al}_3\text{C}_3$ is developed from that of Cr_2AlC . The central idea is the replacement [subfigure (e) over (d)] of Cr atoms at the center of each hexagon with another type of atoms (Hf, in the present case). Stoichiometry-wise, each hexagon in subfigure (e) uniquely includes 1 Hf atom at its center, while leaving 6 Cr atoms at the 6 vertices. But each of these Cr atoms is simultaneously shared by another 2 adjacent hexagons. So for each hexagon, there are $6 \times \frac{1}{1+2} = 2$ Cr atoms. The ratio for Cr and Hf in the crystal is 2:1, hence the chemical formula $(\text{Cr}_2\text{Hf})_2\text{Al}_3\text{C}_3$.

2.2. Computational details

To relax the crystal structure of $(\text{Cr}_2\text{Hf})_2\text{Al}_3\text{C}_3$, we used the Vienna *Ab initio* Simulation Package (VASP)(24-26), with the implementation of the projector-augmented-wave (PAW) approach and the Perdew-Burke-Ernzerhof (PBE) exchange-correlation functional. A high energy cutoff of 600 eV was set for the PAW-PBE potential and a $5 \times 5 \times 2$ k -point mesh was used. The electronic and ionic-force iterations converged to the level of 10^{-5} eV and 10^{-3} eV/Å, respectively. Detailed in figure 2 is the VASP-relaxed crystal structure of $(\text{Cr}_2\text{Hf})_2\text{Al}_3\text{C}_3$. Comparing it with the initial model in figure 1 (f), (g), and (h), the Hf atoms have deviated from the Cr planes and formed new sub-layers, mainly due to their larger atomic radii. Such extrusion of Hf atoms caused the shifting of Al atoms. An example is the Al atom ($x=0.1604$, $y=0.4911$, $z=0.75$) in layer “2” of figure 2, which was originally located at the $x=0$ cell boundary. The overall crystal lattice is also distorted by the atomic size difference. Constants for the new lattice are: $a = 5.1706$ Å, $b = 5.1945$ Å, $c = 12.8104$ Å; $\alpha = \beta = 90^\circ$, $\gamma = 119.8474^\circ$. The elastic constants of $(\text{Cr}_2\text{Hf})_2\text{Al}_3\text{C}_3$ were calculated according to the strain-stress analysis scheme by Nielsen and Martin(27). And the bulk mechanical properties were derived using the Voigt-Reuss-Hill approximation(28-30). The averaged bulk moduli are: 306.86 GPa (Young’s), 125.66 GPa (shear), and 183.32 GPa (bulk), with an averaged Poisson’s ratio of 0.22. These values, along with the energy convergence during the relaxation, suggest that the crystal structure of $(\text{Cr}_2\text{Hf})_2\text{Al}_3\text{C}_3$ is at an energy minimum (structurally stable). To compare its energy with those of its possible competing phases (that have the same chemical composition), additional VASP calculations were performed on two sets of models: a $(\text{Cr}_2\text{Hf})_2\text{Al}_3\text{C}_3$ $1 \times 1 \times 3$ supercell vs. a segregation model and a $(\text{Cr}_2\text{Hf})_2\text{Al}_3\text{C}_3$ $3 \times 3 \times 1$ supercell vs. a solid-solution model. The structures of these two sets of models are shown in figure 3 and figure 4, respectively. And listed in table 1 are the numerical parameters and results of the calculations. Per formula unit, $(\text{Cr}_2\text{Hf})_2\text{Al}_3\text{C}_3$ has an energy of -102.13 eV, lower than that of the segregation (-99.96 eV) and solid-solution (-100.14 eV). This proves that $(\text{Cr}_2\text{Hf})_2\text{Al}_3\text{C}_3$ is more preferable than the segregation and solid-solution, because net energy inputs are needed for Hf atoms in $(\text{Cr}_2\text{Hf})_2\text{Al}_3\text{C}_3$ either to form pure layers (segregation) or to break the order in Cr layers (solid-solution).

2.3. The space group

It is also noticeable from the γ angle in figure 2 that unlike the predecessor, MAX phase, $(\text{Cr}_2\text{Hf})_2\text{Al}_3\text{C}_3$ does not belong to the hexagonal symmetry group anymore. Figure 5 is a plot of the crystal structures with extra colored lines that help illustrate the symmetry group for $(\text{Cr}_2\text{Hf})_2\text{Al}_3\text{C}_3$. In subfigure (a), only when the lattice is rotated by 180° (so that the blue pseudo-rhombus revolves to overlap with the magenta pseudo-rhombus) could the rotated lattice overlap with the original lattice after a $c/2$ translation in the z direction. Any smaller rotation (to the yellow rhombus or green pseudo-rhombus) would not be able to achieve the overlap after translations, because such a rotation would move Hf atoms to the locations originally possessed by Cr atoms. So far it can be determined that the primitive cell has a 2-fold ($360^\circ/180^\circ$) screw axis with a translation of $1/2$ of the c lattice vector. In the Hermann-Mauguin notation, this is denoted as “ $P2_1$ ”. To find possible mirror planes and glide planes for $(\text{Cr}_2\text{Hf})_2\text{Al}_3\text{C}_3$, a look first at Cr_2AlC (the progenitor) would be very helpful. In subfigure (b), there are two mirror planes: the vertical plane in green (crossing C, Al, and Cr atoms) and the horizontal plane in blue (crossing only Al atoms). The crystal structure stays unchanged after reflections of every atom according to either of the mirror planes. Here the structure of Cr_2AlC is Al-terminated, for the purpose of showing the symmetry associated with the horizontal mirror plane. Subfigure (c) shows the glide plane in purple. Reflections of every atom according to this plane result in a structure that needs a $c/2$ translation in the z direction before it can overlap with the original structure. The two mirror planes and one glide plane shown in subfigures (b) and (c) are seen as “ mmc ” in $P6_3/mmc$, the Hermann-Mauguin notation for the space group of Cr_2AlC . From the Al-terminated unit cell of $(\text{Cr}_2\text{Hf})_2\text{Al}_3\text{C}_3$ in subfigure (d), it can be observed that the reflection invariance for the horizontal mirror plane still holds, but that for the vertical mirror plane does not exist anymore. Returning back to subfigure (a), the thin dotted line in green which crosses 4 C atoms indicates the hypothetical vertical mirror plane. It is apparent that Hf and Cr atoms are not mirror images to each other. Meanwhile, a is not equal to b , so they would not be mirror images either even if they were the same type of atoms. A similar reasoning can easily tell that the hypothetical glide plane denoted by the

thin dotted line in purple is not real either. What is left in the case of $(\text{Cr}_2\text{Hf})_2\text{Al}_3\text{C}_3$ is only one horizontal mirror plane. And this leads us finally to the complete Hermann-Mauguin notation: $P2_1/m$ (#11, in the monoclinic space group). With the relaxed structure of $(\text{Cr}_2\text{Hf})_2\text{Al}_3\text{C}_3$, we used the PowderCell program(31) to simulate its X-ray (Cu , $K_\alpha=1.540598 \text{ \AA}$) diffraction pattern, which is plotted in figure6. Such information provides a reference for future experimental confirmations of the phase.

2.4. The electronic density of states

The electronic density of states is also calculated for $(\text{Cr}_2\text{Hf})_2\text{Al}_3\text{C}_3$, using the first-principles orthogonalized linear combination of atomic orbitals (OLCAO) method(32). The total energy was evaluated on a $10 \times 10 \times 4$ k -point mesh in the irreducible portion of the Brillouin zone, and brought to convergence (0.0001 a.u. limit) in 43 iterations. Plotted in figure7 is the electronic density of states for $(\text{Cr}_2\text{Hf})_2\text{Al}_3\text{C}_3$. Like a MAX phase, this material is still metallic. Its total density of states (TDOS) at the Fermi level (E_f) is 18.53 states/(eV·Cell). This fairly large value is primarily due to the relatively large number of atoms (24) in the unit cell. The major contributor to the TDOS at E_f are the Cr-3d states [13.15 states/(eV·Cell)], which can be attributed to the abundance of 3d electrons (5 per Cr atom) and the large number of Cr atoms (8 per unit cell).

4. Conclusions

There are various transition-metal elements available to play the roles of Cr and Hf. And the replacement of the central atom in each hexagon is not restricted to the M site only. The same pattern could be achieved at the A or X site. In addition, this type of phase does not have to be based on a (2 1 1) MAX phase. It could also come from (3 1 2) phases and (4 1 3) phases. This being said, the general formula should be $(\text{M1}_2\text{M2})_{n+1}(\text{A1}_2\text{A2})(\text{X1}_2\text{X2})_n$. Here “M1” and “M2” denote transition-metal elements.

When $M1 \neq M2$, their stoichiometric ratio is 2:1, just like the case for Cr and Hf in $(Cr_2Hf)_2Al_3C_3$; When $M1 = M2$, there is no replacement of M1 (in other words, the M site is pure). Exactly the same usage works as well for A1, A2, and X1, X2. And “ n ” represents the number of stacking layers. These proposed new crystals may inherit a significant portion of wonderful properties from MAX phases, but in the sense of crystallography they represent a new group of materials. We call them “D-MAX” phases because they can have “double” elements at one site. According to their formula, and the possible MAX-phase elements (33) ($M1, M2 = Sc, Ti, Zr, Hf, V, Nb, Ta, Cr, \text{ and } Mo$; $A1, A2 = Cd, Al, Ga, In, Tl, Si, Ge, Sn, Pb, P, As, \text{ and } S$; $X1, X2 = C \text{ and } N$; $n = 1 \text{ to } 3$) from the periodic table, a mathematical permutation and combination analysis suggests that there are 139320 potential D-MAX phases. Obviously, only a small portion of these could actually be synthesized. In the case of their progenitor, MAX phases, a similar analysis would predict that there can be 648 phases, but so far the number of successfully (10) synthesized MAX phases is well below 100. Nevertheless, the present number of MAX phases has already fascinated many scientists and discoveries of new phases continue. We hope our work encourages others to not only experimentally synthesize members of the proposed D-MAX species via powder metallurgy and vapor deposition methods, but also theoretically predict which D-MAX phases, among the vast many, are more likely to be synthesized in pure samples by comparing the energy with that of the associated segregation and solid-solution allotropes.

Acknowledgments

This work was supported by the US Department of Energy (DOE), National Energy Technology Laboratory under Grant No. DE-FE0005865. This research used the resources of the National Energy Research Scientific Computing Center supported by the Office of Basic Science of DOE under Contract No. DE-AC03-76SF00098.

1. Jeitschko W, Nowotny H, Benesovsky F. Carbon-containing ternary compounds (H-phase). Monatshefte fuer Chemie. 1963;94(4):672-6.
2. Jeitschko W, Nowotny H, Benesovsky F. The H-phases Ti_2InC , Zr_2InC , Hf_2InC , and Ti_2GeC . Monatshefte fuer Chemie. 1963;94:1201-5.
3. Bardos DI, Beck PA. Electron phases in certain ternary alloys of transition metals with silicon. Transactions of the Metallurgical Society of AIME. 1966;236(1):64-9.
4. Jeitschko W, Nowotny H. Crystal structure of Ti_3SiC_2 , a new type of complex carbide. Monatshefte fuer Chemie. 1967;98(2):329-37.
5. Wolfsgruber H, Nowotny H, Benesovsky F. Crystal structure of titanium germanium carbide (Ti_3GeC_2). Monatshefte fuer Chemie. 1967;98(6):2403-5.
6. Nowotny H, Benesovsky F. Crystal structures of transition metal carbides and nitrides. Planseeberichte fuer Pulvermetallurgie. 1968;16(3):204-14.
7. Beckmann O, Boller H, Nowotny H, Benesovsky F. Complex carbides and nitrides in the systems Ti-(Zn, Cd, Hg)-(C, N) and Cr-Ga-N. Monatshefte fuer Chemie. 1969;100(5):1465-70.
8. Barsoum MW, El-Raghy T. Synthesis and characterization of a remarkable ceramic: Ti_3SiC_2 . Journal of the American Ceramic Society. 1996;79(7):1953-6.
9. Wang J, Zhou Y. Recent Progress in Theoretical Prediction, Preparation, and Characterization of Layered Ternary Transition-Metal Carbides. Annual Review of Materials Research. 2009 April 28;39:415-43.
10. Sun ZM. Progress in research and development on MAX phases: a family of layered ternary compounds. International Materials Reviews. 2011;56:143-66.
11. Wang X, Zhou Y. Solid-liquid reaction synthesis and simultaneous densification of polycrystalline Ti_2AlC . Zeitschrift fuer Metallkunde. 2002;93(1):66-71.
12. Mo Y, Rulis P, Ching WY. Electronic structure and optical conductivities of 20 MAX-phase compounds. Physical Review B. 2012;86(16):165122.
13. de Rochemont, Pierre L, inventors; Cutting tool and method of manufacture, US Patent 20120012403A1, issued January 19, 2012.
14. Barsoum MW. The $M_{N+1}AX_N$ phases: a new class of solids; thermodynamically stable nanolaminates. Progress in Solid State Chemistry. 2000;28(1-4):201-81.
15. Wang QM, Flores Renteria A, Schroeter O, Mykhaylonka R, Leyens C, Garkas W, et al. Fabrication and oxidation behavior of Cr_2AlC coating on Ti6242 alloy. Surface and Coatings Technology. 2010;204(15):2343-52.
16. Li S, Ahuja R, Barsoum MW, Jena P, Johansson B. Optical properties of Ti_3SiC_2 and Ti_4AlN_3 . Applied Physics Letters. 2008;92(22):221907/1-3.
17. Music D, Sun Z, Schneider JM. Alternating covalent-ionic and metallic bonding in perovskite borides studied using *ab initio* methods. Physical Review B. 2005;71(5):052104.
18. Music D, Schneider JM. Elastic properties of MFe_3N ($M = Ni, Pd, Pt$) studied by *ab initio* calculations. Applied Physics Letters. 2006;88(3):031914-3.
19. Wang J, Zhou Y, Liao T, Lin Z. First-principles prediction of low shear-strain resistance of Al_3BC_3 : A metal borocarbide containing short linear BC_2 units. Applied Physics Letters. 2006;89(2):021917/1-3.
20. Emmerlich J, Music D, Braun M, Fayek P, Munnik F, Schneider JM. A proposal for an unusually stiff and moderately ductile hard coating material: Mo_2BC . Journal of Physics D: Applied Physics. 2009;42(18):185406.
21. Naguib M, Kurtoglu M, Presser V, Lu J, Niu J, Heon M, et al. Two-Dimensional Nanocrystals Produced by Exfoliation of Ti_3AlC_2 . Advanced Materials. 2011;23(37):4248-53.
22. Myhra S, Summers JWB, Kisi EH. Ti_3SiC_2 --A layered ceramic exhibiting ultra-low friction. Materials Letters. 1999;39(1):6-11.

23. Crossley A, Kisi EH, Summers JWB, Myhra S. Ultra-low friction for a layered carbide-derived ceramic, Ti_3SiC_2 , investigated by lateral force microscopy (LFM). *Journal of Physics D: Applied Physics*. 1999;32(6):632-8.
24. Kresse G, Hafner J. *Ab initio* molecular dynamics for liquid metals. *Physical Review B*. 1993;47(1):558-61.
25. Kresse G, Furthmüller J. Efficiency of ab-initio total energy calculations for metals and semiconductors using a plane-wave basis set. *Computational Materials Science*. 1996;6:15-50.
26. Kresse G, Furthmüller J. Efficient iterative schemes for ab initio total-energy calculations using a plane-wave basis set. *Physical Review B*. 1996;54(16):11169-86.
27. Nielsen OH, Martin RM. First-Principles Calculation of Stress. *Physical Review Letters*. 1983;50(9):697-700.
28. Voigt W. *Lehrbuch der Kristallphysik*. Leipzig: Taubner; 1928.
29. Reuss A, Z A. A calculation of the bulk modulus of polycrystalline materials. *Math Mech*. 1929;9.
30. Hill R. The elastic behavior of a crystalline aggregate. *Proceedings of the Physical Society*. 1952;65A:349-54.
31. Gert Nolze, Kraus W. PowderCell. 1998; Available from: http://www.ccp14.ac.uk/ccp/web-mirrors/powdcell/a_v/v_1/powder/e_cell.html.
32. Ching WY, Rulis P. *Electronic Structure Methods for Complex Materials: The orthogonalized linear combination of atomic orbitals*; Oxford University Press; 2012.
33. Michel Barsoum, El-Raghy T. The MAX Phases: Unique New Carbide and Nitride Materials. *American Scientist*. 2001;89(4).

Figures:

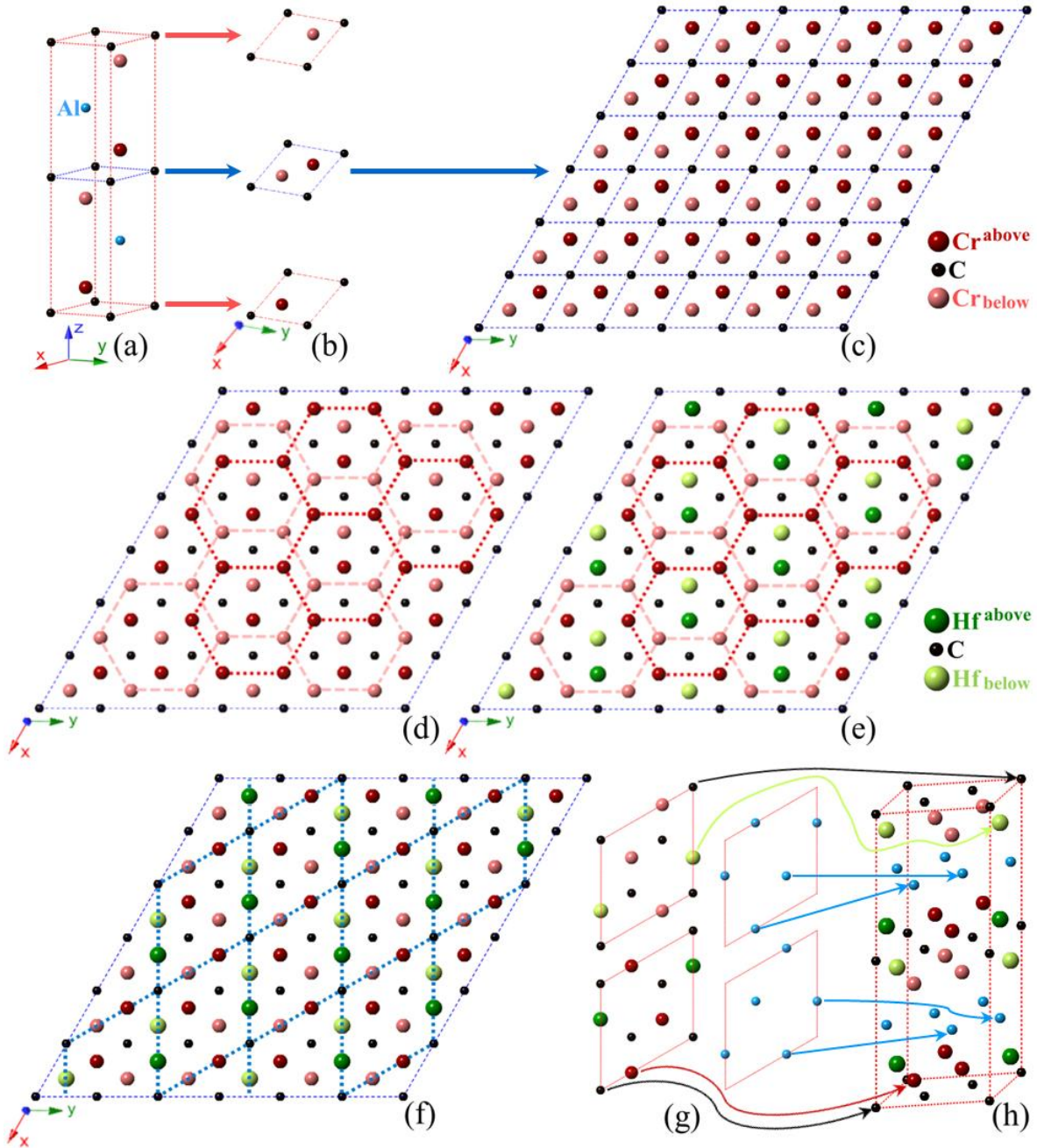


Figure 1. The crystallographic evolution from Cr_2AlC to $(\text{Cr}_2\text{Hf})_2\text{Al}_3\text{C}_3$. (a) is the unit cell of Cr_2AlC . (b) displays Cr-C layers separated from (a). (c) is a 6×6 expansion of the middle layer in (b). (d) has the same structure as that of (c), but with hexagons facilitating the observation of the hexagonal arrangements. (e) shows the structure from (c), with the central Cr atom in each hexagon replaced by Hf. (f) has the same structure as that of (e), but with blue frames indicating the new unit cell. Derived in a similar approach from the top and bottom layers of (b), the left column of (g) shows the other two new layers, and the right column of (g) shows the new Al layers. (h) shows the preliminary unit cell of $(\text{Cr}_2\text{Hf})_2\text{Al}_3\text{C}_3$, assembled with all the cell layers from (g) and (f).

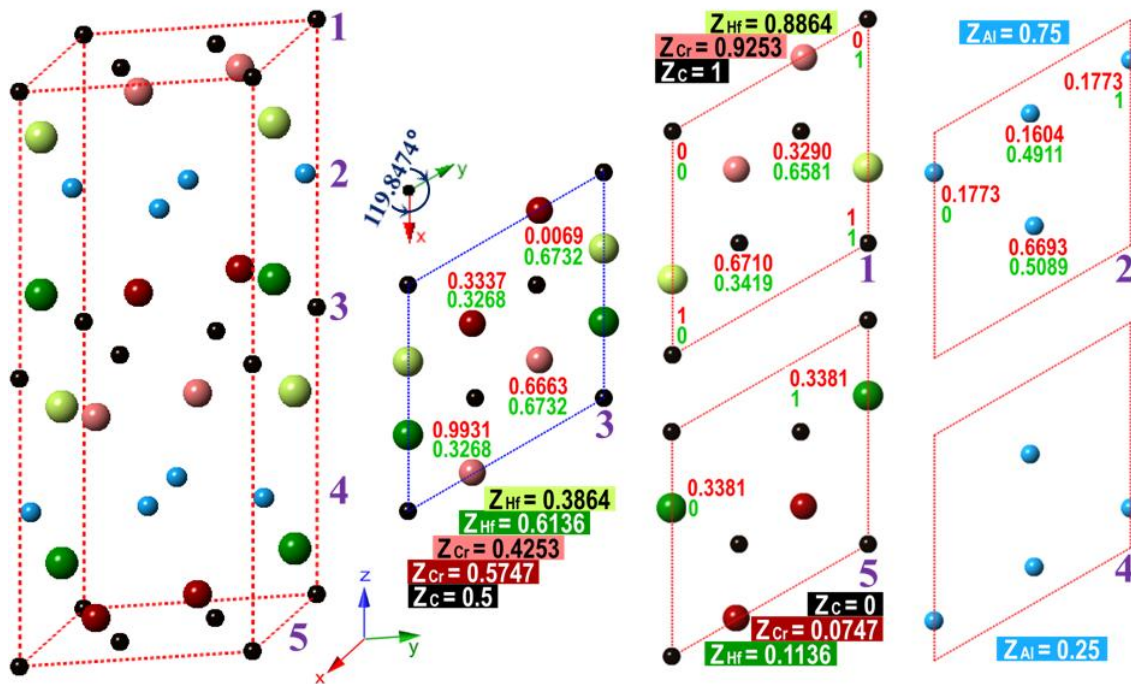


Figure 2. The relaxed crystal structure of $(\text{Cr}_2\text{Hf})_2\text{Al}_3\text{C}_3$. Shown on the left is the unit cell of $(\text{Cr}_2\text{Hf})_2\text{Al}_3\text{C}_3$ with purple numbers “1”, “2”, “3”, “4”, and “5” to its right, marking different layers. And shown on the right are the views of the five layers in the direction from $+z$ to $-z$. Color strips contain the z parameters for each type of atoms. And numbers in red (up) and green (down) are the fractional x and y coordinates for individual atoms. Atoms without coordinates can be easily positioned according to symmetry.

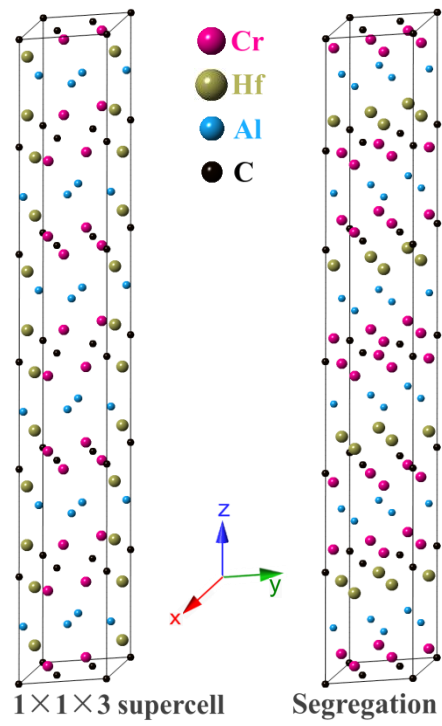


Figure 3. Crystal structures of the $(\text{Cr}_2\text{Hf})_2\text{Al}_3\text{C}_3$ $1 \times 1 \times 3$ supercell and segregation. The purpose of using a supercell is to include enough Hf atoms for the composition of an integer number of pure Hf layers in the segregation model.

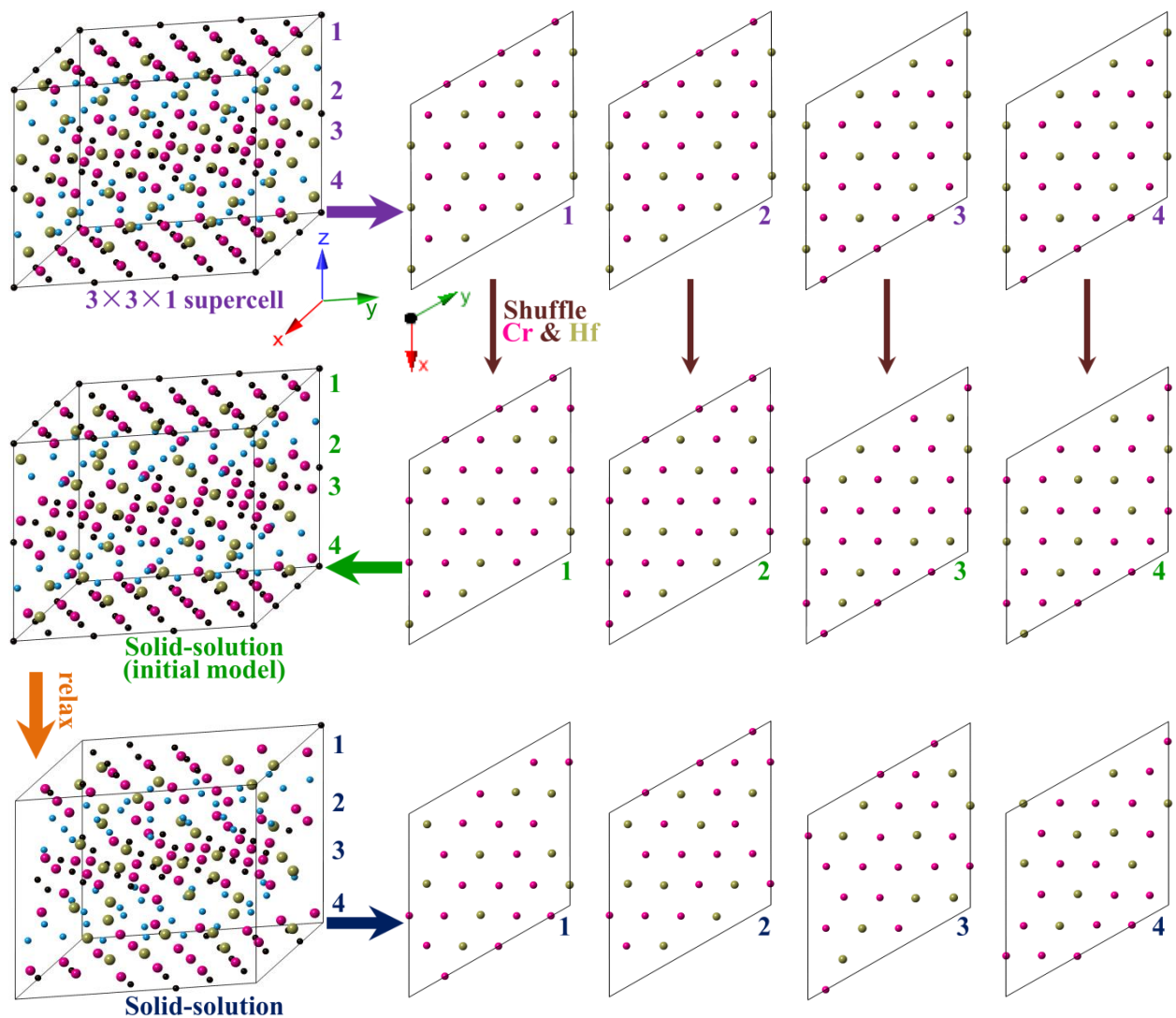
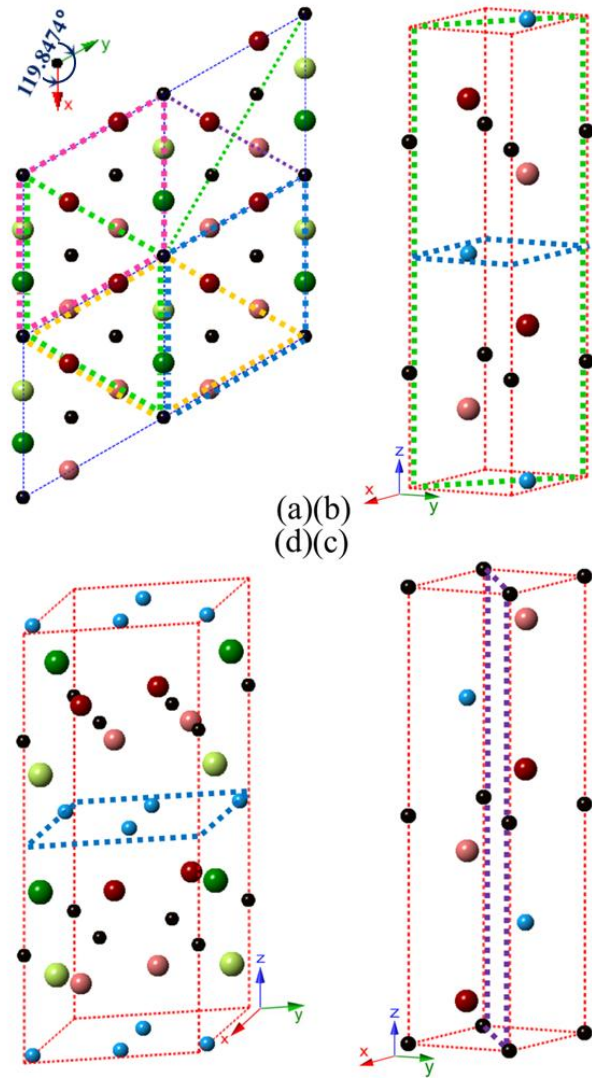


Figure 4. The construction of the solid-solution model based on the $(\text{Cr}_2\text{Hf})_2\text{Al}_3\text{C}_3$ $3 \times 3 \times 1$ supercell. The three-fold duplications in the x and y directions of a unit cell enable the shuffling of the Cr and Hf atoms.



(a)(b)
(d)(c)

Figure 5. The space group symmetry of $(\text{Cr}_2\text{Hf})_2\text{Al}_3\text{C}_3$. (a) is the view (in the direction from $+z$ to $-z$) of a $2 \times 2 \times 1$ supercell of $(\text{Cr}_2\text{Hf})_2\text{Al}_3\text{C}_3$. (b) is the unit cell (Al-terminated) of Cr_2AlC , with two mirror planes in green and blue. (c) is the unit cell of Cr_2AlC , with one glide plane in purple. (d) is the unit cell (Al-terminated) of $(\text{Cr}_2\text{Hf})_2\text{Al}_3\text{C}_3$, with one mirror plane in blue.

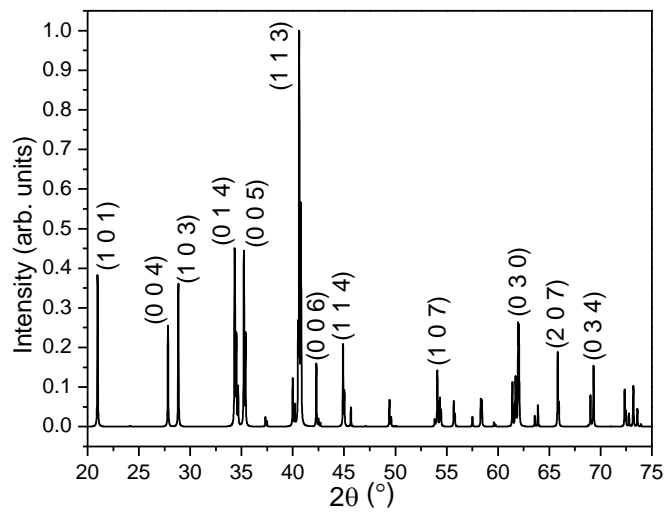


Figure6. Indexed X-ray diffraction pattern of $(\text{Cr}_2\text{Hf})_2\text{Al}_3\text{C}_3$

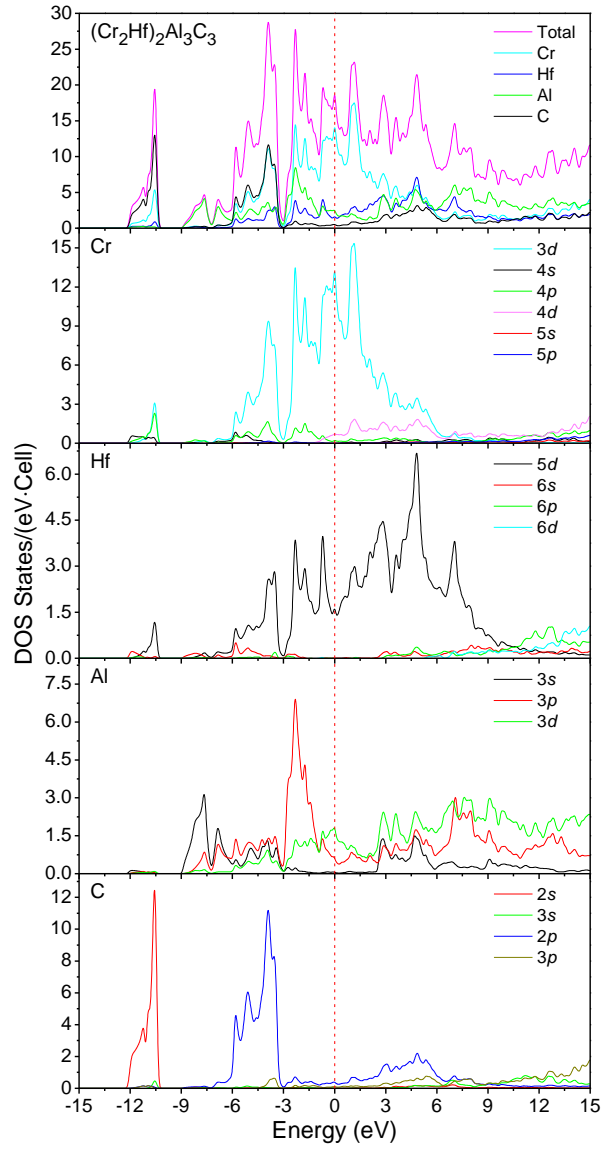


Figure 7. The electronic density of states for $(\text{Cr}_2\text{Hf})_2\text{Al}_3\text{C}_3$. Total and atom-resolved DOS are shown on top, followed underneath by orbital-resolved DOS of each composing element.

Tables:Table 1. Computational configurations and results of $(\text{Cr}_2\text{Hf})_2\text{Al}_3\text{C}_3$ supercells and corresponding models of segregation and solid-solution.

	1×1×3 supercell	Segregation	3×3×1 supercell	Solid-solution
Number of atoms	72	72	216	216
<i>k</i> -point mesh	5×5×1	5×5×1	2×2×2	2×2×2
Convergence (eV/Å)	electronic	10 ⁻⁵	10 ⁻⁵	10 ⁻⁵
	ionic-force	10 ⁻³	10 ⁻³	10 ⁻³
Total energy (eV)	per cell	-612.76	-1838.25	-1802.48
	per formula unit	-102.13	-102.13	-100.14
Lattice constants	<i>a</i> (Å)	5.17	15.51	15.60
	<i>b</i> (Å)	5.20	15.59	15.60
	<i>c</i> (Å)	38.40	39.63	13.24
	<i>α</i> (°)	90.00	90.00	89.64
	<i>β</i> (°)	90.00	90.00	90.55
	<i>γ</i> (°)	119.84	120.00	120.04